Imaging Approach to Mechanistic Study of Nanoparticle Interactions with the Blood–Brain Barrier

Mattia Bramini, Dong Ye, Anna Hallerbach, Michelle Nic Raghnaill, Anna Salvati,[†] Christoffer Åberg,[‡,*] and Kenneth A. Dawson[*]

Centre for BioNano Interactions, School of Chemistry and Chemical Biology & UCD Conway Institute for Biomolecular and Biomedical Research, University College Dublin, Belfield, Dublin 4, Ireland. [†]Present address: Groningen Research Institute of Pharmacy, Groningen University, Antonius Deusinglaan 1, 9713 AV Groningen, The Netherlands. [‡]Present address: Groningen Institute of Biomolecular Sciences & Biotechnology, Groningen University, Nijenborgh 4, 9747 AG Groningen, The Netherlands.,

ABSTRACT

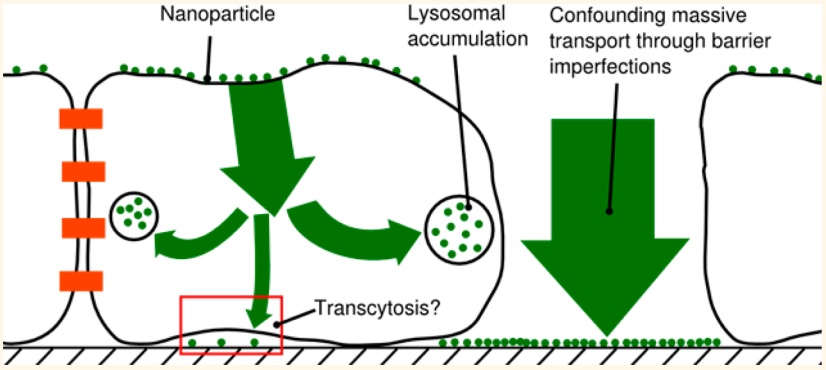

Understanding nanoparticle interactions with the central nervous system, in particular the blood–brain barrier, is key to advances in therapeutics, as well as assessing the safety of nanoparticles. Challenges in achieving insights have been significant, even for relatively simple models. Here we use a combination of live cell imaging and computational analysis to directly study nanoparticle translocation across a human *in vitro* blood–brain barrier model. This approach allows us to identify and avoid problems in more conventional inferential *in vitro* measurements by identifying the catalogue of events of barrier internalization and translocation as they occur. Potentially this approach opens up the window of applicability of *in vitro* models, thereby enabling in depth mechanistic studies in the future. Model nanoparticles are used to illustrate the method. For those, we find that translocation, though rare, appears to take place. On the other hand, barrier uptake is efficient, and since barrier export is small, there is significant accumulation within the barrier.

KEYWORDS: blood–brain barrier · nanoparticle · transcytosis · lysosome · live-cell imaging · confocal microscopy · TIRFM

Passage across the capillaries in the brain and the central nervous system is tightly regulated by a structure known as the blood–brain barrier.[1,2] Nanoparticle sizes are such that they are internalized by engaging with endogenous cellular pathways.[3−5] For this reason they may be able to access the central nervous system through the blood–brain barrier, raising questions on their safety[6] but also giving hope on achieving more efficient drug delivery into the brain.[7−10] Indeed, nanoparticles have been found in the brain following inhalation exposure,[11,12] though the detailed mechanisms in crossing the blood–brain barrier remain uncertain, possibly in some cases involving the olfactory nerve.[12] Nanoparticles have also proven successful at delivering drugs across the blood–brain barrier after intravenous injection,[13] though a proposed mechanism is that the drug is released from the nanoparticles inside the blood–brain barrier and passes into the brain unassisted.[7] It has been suggested that either adsorbed or covalently linked endogenous proteins (such as apolipoprotein E[13−17] and transferrin[18,19]) or peptides (such as RVG29[20] or Angiopeps[21]) on the nanoparticle surface may mediate uptake into the barrier both *in vitro*[14,15,19,21]

* Address correspondence to Kenneth.A.Dawson@cbni.ucd.ie; Christoffer.Aberg@cbni.ucd.ie.

Received for review November 13, 2013 and accepted April 24, 2014.

Published online April 28, 2014
10.1021/nn5018523

© 2014 American Chemical Society

and *in vivo*.[13,16−18,20,22] Additionally, highly charged cationic objects have been grafted to seek a strong adsorption to the plasma membrane followed by unspecific internalization (adsorptive mediated transcytosis).[23] The details can, however, be rather subtle. Thus, nanoparticles in realistic biological fluids (which, naturally, include *in vivo* conditions) often adsorb to their surface biomolecules present in the medium, forming a so-called biomolecular corona, which modulates the subsequent interactions.[24] Concomitant with this corona formation, loss of specificity of the targeted nanoparticles may occur.[25] On the other hand, the same general mechanism (assisted by prior surfactant coating) has been reported to adsorb apolipoprotein E, thus leading to an effective targeting,[16,17,22] *i.e.*, the opposite outcome.

Without doubt, *in vivo* studies remain central to the development of this whole arena, but *in vitro* models (providing they are sufficiently faithful in representing relevant processes) combined with the right tools potentially open up quite novel mechanistic insights that are highly desirable. At times, we believe, commonly identified deficits in simple blood−brain barrier cellular models (in their study of nanoparticle interactions) may result from a complicated mixture of absent biological function, imperfect maturation, or growth of the layer, as well as defects of the barrier, and the supporting matrix. All of these are difficult, complex, and poorly understood issues—whether *in vivo* or *in vitro*—and the lack of good interpretive tools in the *in vitro* models has made it difficult to satisfactorily assess the value of such models for nanoparticle studies.

In particular, we believe that although *in vitro* models may possess various defects and gaps on larger scales, they can retain important biological mechanisms, relevant for nanoparticle interactions, in localized patches, provided these can be usefully studied. Here, using a combination of spinning-disk confocal microscopy and total internal reflection fluorescence microscopy for both direct three-dimensional and high-speed imaging of a living barrier we investigate such patches. Thus, we are able to map the spatiotemporal behavior of proteins and nanoparticles inside the barrier and identify relevant functions. This approach goes beyond those traditional methods (developed for molecular studies) for *in vitro* barriers that measure transport through a macroscopic sample, allowing some of the deficits of the models to be overcome and details of the barrier transport mechanism to be unveiled.

RESULTS AND DISCUSSION

Immortalized human brain capillary microvascular endothelial hCMEC/D3 cells[26] acted as an *in vitro* blood−brain barrier model. Fluorescently labeled transferrin protein was used as a control, and 40 and 100 nm (nominal diameter) carboxylated polystyrene (PS-COOH) nanoparticles were used as particle models because they are dispersible in the appropriate cell culture medium (Table 1) and we have previous experience of their uptake and intracellular location in other cell types.[5,27,28] Additionally, they do not impede cell viability at the concentrations and time scales used in this study.[29]

TABLE 1. Physicochemical Characterization of the Nanoparticles Used in the Study

sample	medium	T (°C)	diameter[a] (nm)	PDI[b]	ζ-potential (mV)
40 nm PS-COOH	PBS	25	59 ± 2	0.14	−30 ± 1
40 nm PS-COOH	EBM-2	37	76 ± 1	0.1	−12 ± 1
100 nm PS-COOH	PBS	25	108 ± 1	0.06	−35 ± 1
100 nm PS-COOH	EBM-2	37	122 ± 2	0.34	−13 ± 1

[a] *z*-Average hydrodynamic diameter extracted by cumulant analysis of the data. [b] Polydispersity index from cumulant fitting of the data.

The hCMEC/D3 cells were cultured for 7 days to form a barrier, as described in previous literature.[30,31] During the first few days, the cells divide and become confluent. *In vivo*, neighboring cells in physical contact form so-called "tight junctions", impermeable protein complexes between adjacent cells, which ensure that no transport occurs between the barrier cells. In the *in vitro* model, tight junctions form progressively and mature after 7 days (Supporting Figure S1). The typical macroscopic determinants for our barrier models are comparable to previous reports (transendothelial electrical resistance, *etc.*) and have been determined for the protocol used here, as reported elsewhere.[31]

However, to further assess the biological functionality of the barrier, it was exposed to fluorescently labeled transferrin protein (Supporting Figures S2−4 and Video S1), which has been suggested to undergo barrier crossing (possibly transcytosis) through the blood−brain barrier,[32] though the detailed mechanism is not clearly defined in the literature.[2] Certainly there is limited evidence from Transwell systems that a temperature-dependent transport process for transferrin does exist (Supporting Figure S5). Now, however, within matured barriers we observed transferrin move in highly transient tubular structures (some shorter tracks) with no obvious particular orientation (Supporting Figure S2 and Video S1), combined with more extended channels through the barrier that are relatively long-lived (Supporting Figure S2), potentially providing continuous active pathways for transferrin across the model barrier. Such processes are only very rarely observed for individual hCMEC/D3 cells cultured for only 2−3 days (Supporting Figure S3). This suggests an emergent barrier crossing function that is present within these barriers, developing in parallel with the reformation of relevant junctions (Supporting Figure S1). Obviously, given how little is known about the mechanism of *in vivo* barrier crossing, there is no way to

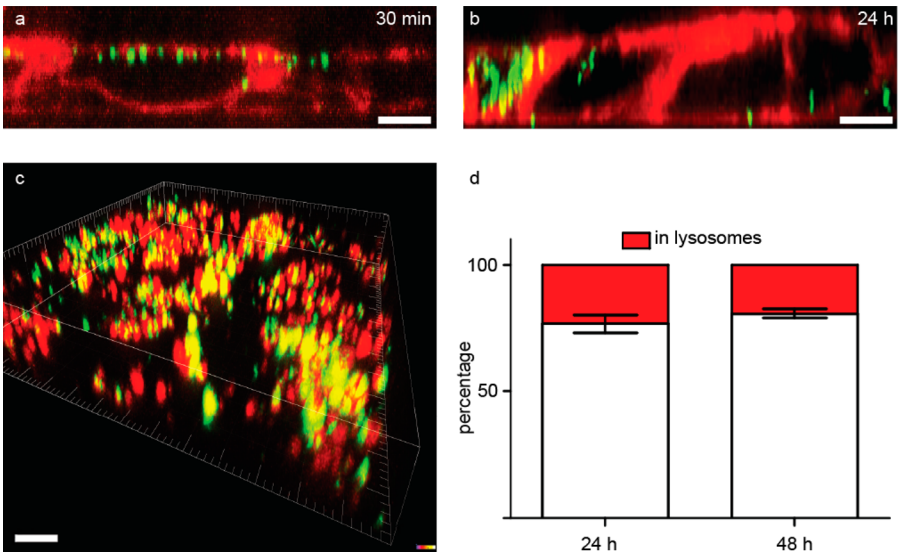

Figure 1. Uptake and subcellular location of 100 nm PS-COOH in the *in vitro* blood−brain barrier model. (a, b) Cross-section of barriers 30 min and 24 h after a 10 min nanoparticle exposure, obtained using spinning-disk confocal fluorescence microscopy (scale bar 3 μm). Nanoparticles (green) are observed on the upper (apical) cell membrane (CellMask; red) in panel a; in panel b nanoparticles have entered the cells, some nanoparticles being found at the lower (basolateral) cell membrane. (c) 3D rendering of nanoparticles (green) and lysosomes (LysoTracker Red; red) in the barrier 24 h after a 10 min nanoparticle exposure (scale bar 5 μm). Yellow corresponds to nanoparticles close to (co-localized with) lysosomes. See also Supporting Video S3, showing the comovement of a nanoparticle with a lysosome, and Supporting Figure S11 for a corresponding image from electron microscopy. (d) Proportion of nanoparticles inside lysosomes 24 and 48 h after the 10 min exposure. Results are presented as mean ± standard deviation over three independent experiments (see Supporting Figures S9 and S10 for details).

prove that this renders the present model satisfactory. Still, it is a significant and clear outcome and makes it worth studying in more detail the nature of nanoparticle−barrier interactions.

It is important to note, though, that from a more macroscopic point of view, and in numerous surfaces and supports (such as Transwell membranes),[33] one can find many local imperfections in the barrier, such as bi- or multilayers (Supporting Figure S6) or holes and gaps (Supporting Figures S7, S8 and Video S2), in the *in vitro* model. These have been studied in some depth, and we note that such imperfections have considerable implications for macroscopic barrier crossing of nanoparticles. Thus, for the cases we consider, true biologically mediated nanoparticle crossing is so slow that one may often see mainly the effects of such barrier defects in macroscopic measurements. Indeed, it is interesting to note that we can even estimate the density of barrier defects from the imaging, and then a simple model (see Supporting Information) suggests that macroscopic experiments on nanoparticles would largely be measuring transport through holes in the barrier, rather than *via* active processes through the barrier cells. When these issues are combined with other detailed challenges, such as the effects on particle transport by the nature of the Transwell supports,[33] one observes the benefit of being able to study such models more locally. Thus, in order to study actual cell-barrier crossing (rather than passage through holes and defects), we choose to image and investigate only apparently well-functioning domains of the *in vitro* model. The remainder of this study shows results coming solely from such domains.

The uptake and subcellular location of the nanoparticles were investigated by exposing the *in vitro* blood−brain barrier model (cultured for 7 days until tight junction formation) to 100 nm PS-COOH nanoparticles (100 μg/mL in cell culture medium) for 10 min, washing with (nanoparticle-free) buffer, and incubating further in nanoparticle-free medium. To follow the nanoparticles inside the barrier, cell membranes were stained (CellMask) and the barrier was imaged in three dimensions using spinning-disk confocal fluorescence microscopy. Using the cell membrane stain, we can avoid investigating areas with obvious defects (Supporting Figure S6−8) and focus attention on patches of intact barrier. All individual events in a field of view (typically consisting of 5−7 barrier cells) of the intact barrier may thus be followed by confocal microscopy, in considerable detail. Immediately after washing, nanoparticles were found closely associated with the upper (apical) cell membrane (Figure 1a), likely adhering outside the barrier, but with time they progressively entered the barrier (Figure 1b).

We stress that it is clear from the images that the majority of nanoparticles (when one observes well-functioning cellular domains) does not pass intact parts of the barrier even 48 h postexposure, but ends up in intracellular organelles, many of them lysosomes, similarly to several other nanoparticle/cell line systems.[3,5,28] As far as we can tell (in line with other recent experimental evidence[27]), there is limited or no recycling of

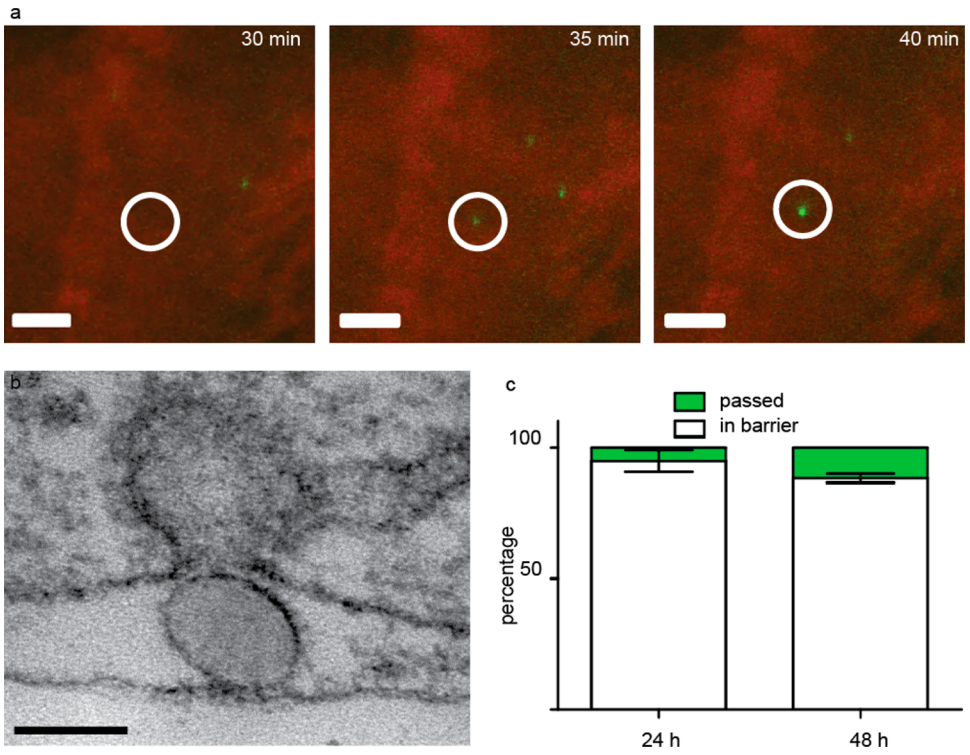

Figure 2. Translocation of 100 nm PS-COOH nanoparticles across the *in vitro* blood–brain barrier model. (a) Dual-color TIRFM 30–40 min after the 10 min nanoparticle exposure (scale bar 3 μm). A nanoparticle (green; white circle) can be seen approaching the cell membrane after 35 min and becomes immobile after 40 min, potentially after having passed to the outside of the cell and adhering on the glass below the barrier. Supporting Figure S12 shows another example, and Supporting Videos S4 and S5 show the processes. (b) Electron microscopy image of a nanoparticle between the lower (basal) cell membrane and the support filter, in close proximity to a membrane invagination (scale bar 100 nm). See Supporting Figure S11 for the full image. (c) Proportion of nanoparticles immobile at the lower cell membrane ("passed") 24 and 48 h after the 10 min exposure. Results are presented as mean ± standard deviation over at least three independent experiments (see Supporting Figures S15 and S16 for details).

these particles and they accumulate within the barrier. Thus, acidic organelles were fluorescently labeled with an acidotropic dye (LysoTracker Red), before the 10 min nanoparticle exposure, subsequent washing, and further incubation in nanoparticle-free medium for 24 and 48 h prior to imaging. A significant number of nanoparticles are observed associated with lysosomes (Figure 1c and Supporting Video S3). The number of such nanoparticles was quantified as the number of nanoparticles within 0.5 μm from a LysoTracker-labeled object and averaged over fields of view (Supporting Figures S9 and S10 show that the averages are representative; see Methods for further details). Even if between independent experiments exact reproducibility was difficult to achieve, both for the total number of nanoparticles and the number of nanoparticles considered to be in lysosomes (Supporting Figures S9 and S10), the fraction of lysosomal accumulation was quite well-determined. After 24 h, the degree of lysosomal accumulation was around 20% (Figure 1d), indicating that a significant fraction of nanoparticles accumulates in lysosomes, as confirmed also by electron microscopy (Supporting Figure S11). Interestingly, the degree of lysosomal accumulation did not increase between 24 and 48 h (Figure 1d), suggesting that reaching the lysosomes occurs within the first 24 h, although one should keep in mind that our quantification does not take into account that several nanoparticles inside a lysosome (*cf.* Supporting Figure S11) may be identified as a single fluorescent object due to the resolution limit of light microscopy.

Also within the seemingly well-functioning domains, there is no doubt that some particles do make significant excursions across the whole barrier, approaching the basal side (Figure 1b). The methodology described here also allows us to image appearances of nanoparticles below the barrier, to at least address the much discussed issue of whether nanoparticles can fully access barrier-crossing pathways. Thus, total internal reflection fluorescence microscopy (TIRFM) provides an improved resolution in a thin (on the order of a few hundred nanometers) section close to the glass (*i.e.*, the lower, basolateral, side of the barrier) and was used to monitor eventual transcytosis immediately after nanoparticle exposure, in real time. TIRFM showed rare appearances of nanoparticles below the barrier (Figure 2a, Supporting Figure S12 and Videos S4 and S5); similar events were also found using confocal microscopy (Supporting Figure S13 and Video S6). Furthermore, a snapshot, apparently of the same type of process, was caught using electron microscopy (Figure 2b and Supporting Figure S11).

To estimate the occurrence of such events, we acquired several (up to 20) different fields of view of barriers 24 and 48 h after nanoparticle exposure. Only domains of the barrier without obvious defects were considered. Nanoparticles close to the lower (basolateral) side that did not move during 25 consecutive three-dimensional images ("*z*-stacks") were identified. The optical resolution limit does not allow an unequivocal determination of whether such nanoparticles are actually outside the barrier. However, intentionally disrupting the barrier (using phototoxic damage induced by prolonged exposure to laser irradiation) showed that the nanoparticles on the lower (basolateral) side did not follow the rest of the cell when it reacted to the damage (Supporting Figure S14 and Videos S7 and S8), thus suggesting that they are extracellular. The translocation ratio was estimated as the number of such nanoparticles on the bottom of the barrier to the total number of nanoparticles, both averaged over several fields of view (Supporting Figures S15 and S16 show that the averages are representative; see Methods for further details). It is clear that the proportion of translocated particles is rather low and usually at most several percent, even after 48 h (Figure 2c).

Since nanoparticles are actively taken up by cells, one may expect a strong size-dependence based on the known size ranges of the endocytic mechanisms.[34] Although a clear answer on the detailed uptake mechanism of nanoparticles remains elusive,[35] an optimum size range for uptake into single cells has indeed been reported.[4] The size-dependence of translocation is, however (to our knowledge), less established, so we applied our methodology also to a smaller nanoparticle of the same material, 40 nm PS-COOH, at the same concentration (in number of nanoparticles per unit volume). The results were largely similar, with a significant lysosomal accumulation and low amount of barrier translocation, when only considering intact patches of the barrier (Supporting Figure S17). PS-COOH of 40 nm seems to pass the *in vitro* blood brain−barrier to a somewhat higher extent compared to 100 nm PS-COOH (Supporting Figure S17), but the basic conclusion remains that translocation is a rare event.

It is perhaps worth mentioning that our experiments have been carried out at relatively high particle concentrations, and this is reflected in the levels of intrabarrier accumulation observed. We also carried out a limited study at lower concentrations to investigate possible effects on the ratio of intracellular accumulation *versus* translocation. Ten- and hundred-fold lowered doses (1 and 10 μg/mL compared to 100 μg/mL) of 100 nm PS-COOH were exposed to the barrier, and translocation and lysosomal accumulation assessed as above. We could not conclude any major concentration-dependence, neither in lysosomal accumulation nor in passage ratio (Supporting Figures S18−20), at least at these concentrations.

It is important to interpret the low translocation rate in light of imperfections of the barrier. Even after tight junction formation and for the intact patches we investigated, over such very long periods barrier cells could still in principle move and change shape significantly (Supporting Figure S21), and it is not feasible to continuously follow at sufficient time resolution the whole course of events. We can, therefore, not exclude the possibility that nanoparticles found below an intact barrier actually passed through a temporary hole, which subsequently "healed" between nanoparticle exposure and imaging. Nor can we rule out microscopic holes below the optical resolution limit; for example, it appears as if transferrin, though much smaller, is able to pass through holes in the barrier (Supporting Figure S22). Still, collectively, the evidence of particle movement in the barrier and the information above (including snapshots from electron microscopy) do suggest that such true barrier crossing events occur. Nevertheless, their proportion is very small compared to the different modes of barrier accumulation observed, which evidently could have significant practical implications, if this is indeed reflective of *in vivo* situations.

CONCLUSIONS

In summary, we have augmented previous studies of nanoparticle translocation through the blood−brain barrier with a live-cell imaging investigation on an *in vitro* model. Crucially, this methodology allows us to determine with high levels of confidence how the particles interact with barriers that possess barrier crossing functionality. A major advantage of the approach is that the full spatiotemporal evolution of the nanoparticles inside the barrier can be directly followed, thus enabling us to study nanoparticle behavior from their early entry to their final localization. In particular, we were able for the first time to identify and show candidate events of nanoparticles translocating across the barrier and to see the events occurring "live", using both spinning-disk confocal microscopy and total internal reflection fluorescence microscopy. Nevertheless, barrier translocation is at most a rare event for the model nanoparticles used in this study, and most nanoparticles remain in the barrier, with a significant portion accumulating in the lysosomes without evident clearance (providing they do not degrade). This is significant, as common macroscopic methods of isolating blood−brain barrier samples for biodistribution analysis are not capable of resolving in-barrier and cross-barrier accumulation, so one should be cautious in their interpretation.

The potential hazard implication of nanoparticle−barrier association (rather than barrier crossing) has also arisen in recent discussions where nanoparticles may even remain outside the barrier, but still induce signaling processes.[36,37] We comment that nanoparticle

accumulation in the blood−brain barrier itself is a significant additional mode for this to occur. The long-term consequences of the significant lysosomal accumulation shown here may also need to be addressed. Moreover, the fate and potential impact of the nanoparticles that neither translocate nor accumulate in lysosomes but within other intracellular vesicles remain to be investigated.

The advantages of being able to carry out full mechanistic and imaging studies with *in vitro* models are significant, if indeed the models themselves are of value. We stress that such models need not accurately reflect all aspects of real barriers, but merely retain sufficient (relevant) functionality for specific studies. The imaging and analysis approach used here allows the explicit assessment of the presence of the most obvious imperfections, and one can thereby refrain from investigating affected regions. Such microscopic understanding raises the question of whether macroscopic parameters of barrier models (for example from Transwell membranes) are fairly representing the potential of *in vitro* models to contribute to the nanoparticle−barrier question. We believe that a re-evaluation of the potential for mechanistic *in vitro* and *in vivo* studies to complement each other may be feasible. This could be a very fruitful axis of collaboration, because the effects of nanoparticle properties on translocation propensity are sometimes subtle and complex; if such effects could be investigated *in vitro*—with confidence—then costly and time-consuming *in vivo* studies may be limited to validation or studies of particular significance. For example, the role of lipoproteins (whether adsorbed[14,16,17,22] or grafted[13,15]) may be more easily clarified in an *in vitro* setup, where serum and lipoprotein concentrations can be varied at ease. In general, an established *in vitro* methodology may pave the way for an increased understanding and exploration, in particular for nanoparticle-based therapeutic delivery to the brain.

METHODS

Cell Culture. Immortalized human brain capillary endothelial hCMEC/D3 cells were used in passages 7−10. For culturing, 10^6 cells were seeded in a collagen-coated flask (25 cm^3, Becton Dickinson) and supplemented with EBM-2 medium containing vascular endothelial growth factor (VEGF), insulin-like growth factor-1 (IL-1), epidermal growth factor (EGF), basic fibroblast growth factor (bFGF), fetal calf serum (2%), gentamicin sulfate/amphotericin B, and hydrocortisone (Lonza Biosciences). For nanoparticle experiments, cells were supplemented with growth factor depleted EBM-2 assay medium containing bFGF, 2% fetal calf serum, hydrocortisone, and 10 mM HEPES during monolayer formation (7 days). Cells were cultured in an incubator at 37 °C with 5% CO_2/95% air and saturated humidity. Cell culture medium was changed every 2 days, and monolayer medium twice weekly.

Nanoparticle Characterization. Carboxylated polystyrene (PS-COOH) nanoparticles of 40 and 100 nm (nominal diameters) were purchased from Invitrogen (Life Technologies, Carlsbad, CA, USA). The size of the nanoparticles dispersed in phosphate-buffered saline (PBS) solution (Gibco, Invitrogen) and assay media (EBM-2, Gibco, Invitrogen) was determined by dynamic light scattering (DLS) using a Malvern Zetasizer 3000HSa (Malvern Instruments Ltd., Worcestershire, UK). The particles were diluted in 1.5 mL of PBS and assay medium to reach a 100 μg/mL concentration. The solutions of particles were incubated at 37 °C in an orbital shaker over 4 h and sampled each hour. The measurements were conducted at 37 °C by transferring 500 μL of the stock solution to a square cuvette for DLS analysis. DLS results are the average of a minimum of three separate runs and are reported in Table 1; errors represent the standard deviation over measurements and are intended solely as an indication of the reproducibility of the measurement.

The effective surface charge (zeta potential) of the nanoparticles was also measured in both PBS and assay medium using a Malvern Zetasizer 3000HSa (Malvern Instruments Ltd., Worcestershire, UK). The solutions of particles were incubated at 37 °C in an orbital shaker over 4 h and sampled each hour. The measurements were conducted at 37 °C by transferring 500 μL of the stock solution to a square cuvette for zeta potential measurements. In PBS, the zeta potential of both 40 and 100 nm nanoparticles is strongly negative, but in medium, in the presence of serum proteins, the zeta potential tends to neutrality. Zeta potential results are the average of a minimum of three separate runs and are reported in Table 1; errors represent the standard deviation over measurements and are intended solely as an indication of the reproducibility of the measurement.

Confocal Microscopy. For confocal microscopy, 2×10^5 cells were seeded onto 35 mm plates with 15 mm diameter glass coverslips and grown for 3, 4, 5 and 7 days until monolayer formation. For organelle and protein staining, samples were washed three times with 1 mL of PBS, fixed for 4 min with 1 mL of 100% methanol at −20 °C, and incubated for 30 min at room temperature with a blocking solution of 1% bovine serum albumin fraction V (Sigma-Aldrich, St. Louis, MO, USA) in PBS-Tween to prevent nonspecific binding. Samples were then incubated for 1 h at room temperature with a primary antibody 1:100 rabbit polyclonal to claudin-5 (Abcam, Cambridge, UK), washed three times with 1 mL of PBS, and then incubated at room temperature for 1 h with a 1:500 dilution of AlexaFluor 546 goat anti-rabbit IgG (claudin-5) as a secondary antibody (Molecular Probes, Life Technologies, Carlsbad, CA, USA). Samples were washed three times with 1 mL of PBS and incubated for 5 min with DAPI (Sigma-Aldrich, St. Louis, MO, USA) before mounting with MOWIOL (Polysciences Inc., Warrington, PA, USA) on slides for imaging. The cells were observed using a Carl Zeiss LSM 510 Meta laser scanning confocal microscope (Zeiss, München, Germany) with lasers at 364 nm (DAPI) and 547 nm (claudin-5 antibody).

Spinning-Disk Confocal Microscopy. For spinning-disk confocal microscopy, 25×10^3 cells were seeded onto four-well live-chamber slides (LabTek, Thermo Scientific, Waltham, MA, USA) and grown for 7 days before carrying out the experiment (2 days for single-cell experiments with fluorescently labeled transferrin and Alexa488 dye). The four-well live chamber was coated with 0.5 mL of collagen (0.1 mg/mL rat tail collagen type 1, Sigma) on the day of seeding and incubated at 37 °C in a sterile incubator over 30 min. Each well was washed three times in PBS and allowed to dry for 30 min. hCMEC/D3 cells were seeded in 0.7 mL of growth factor depleted EBM-2 assay medium at a density of 25×10^3 cells/well. Medium was replaced 6 h postseeding and then only once during the 7 days of barrier formation. The day of the microscopy acquisition, live cells were stained with different organelle dyes in assay medium at 37 °C and washed before image acquisition or exposure to the nanoparticles. The concentrations and incubation times were as follows: LysoTracker Red (Molecular Probes) at 0.10 μM for 1 h and CellMask (Molecular Probes) at 7.5 μg/mL for 5 min. For experiments with nanoparticles, particle dispersions were prepared in assay medium at 37 °C prior to addition to the cells. Cells were exposed to nanoparticle dispersions at different

concentrations (1, 10, and 100 μg/mL) for 10 min. After particle exposure, medium was removed and samples were washed three times with PBS, also at 37 °C. Fresh assay medium at 37 °C was then added to the cells, and these were taken to the microscope, where the imaging was done at 37 °C in 5% CO_2 and 60% relative humidity.

For the experiment with transferrin protein, fluorescently labeled (Alexa488) transferrin (Invitrogen) dispersions were prepared in serum-free assay medium at 37 °C prior to addition to cells. Cells were exposed to a 5 μg/mL transferrin solution for 30 min. After transferrin exposure, medium was removed and samples were washed three times with PBS, also at 37 °C. Fresh assay medium at 37 °C was then added to the cells, and the imaging was done at 37 °C in 5% CO_2 and 60% relative humidity. The same experimental conditions and concentration, in mass per unit volume, were used for the imaging of cells exposed to Alexa488 dye (the usage of the same mass concentration implies that the number concentration was higher for the dye).

Dual-color visualization of cell organelles, nanoparticles, transferrin, and Alexa488 dye was performed on a spinning-disk confocal microscopy system consisting of a CSU22 spinning-disk unit (Yokogawa Electric Corporation) and an Andor iXon3 897 EMCCD camera (Andor, Belfast, UK), mounted on an inverted fully motorized Olympus IX81 microscope body (Olympus Corporation, Tokyo, Japan) with climate control chamber. The nanoparticles, the transferrin protein, and the Alexa488 dye were excited with a 488 nm laser line, and Draq5, LysoTracker Red, and CellMask were excited using a 561 nm laser line. A CFI Plan Apo 100×/1.4 WD = 0.13 mm oil immersion objective was used (Olympus). Images were acquired using Andor iQ software and processed using Imaris imaging software (Bitplane AG, Zurich, Switzerland).

Total Internal Reflection Fluorescence Microscopy. For TIRFM, 25×10^3 cells were seeded onto four-wells live-chamber slides (LabTek) and grown for 7 days before carrying out the experiment. The four-well live chamber was coated with 0.5 mL of collagen (0.1 mg/mL rat tail collagen type 1, Sigma) on the day of seeding and incubated at 37 °C in a sterile incubator over 30 min. Each well was washed three times in PBS and allowed to dry for 30 min. hCMEC/D3 cells were seeded in 0.7 mL of growth factor depleted EBM-2 assay medium at a density of 25×10^3 cells/well. Medium was replaced 6 h postseeding and then only once during the 7 days of barrier formation. The day of the microscopy acquisition, live cells were stained with CellMask (Molecular Probes) at 7.5 μg/mL for 5 min in assay medium at 37 °C and washed away before taking the cells to the microscope and adding the fluorescently labeled transferrin. Fluorescently labeled transferrin dispersion was prepared in serum-free assay medium at 37 °C prior to addition to the cells. TIRFM image acquisition was started before adding the transferrin solution to the cells, when only the CellMask staining could be detected. Using the Nikon Perfect Focus System to keep the sample in focus for the whole duration of the experiment, cells were then exposed to 5 μg/mL transferrin solution while dual-color TIRFM acquisition was already occurring. The imaging was done at 37 °C in 5% CO_2 and 60% relative humidity. The same protocol and procedure were followed to investigate the nanoparticles' (100 nm PS-COOH at a concentration of 100 μg/mL) passage through holes (imperfections) in the hCMEC/D3 monolayer. The live nanoparticle translocation through the *in vitro* blood–brain barrier model was also investigated using TIRF microscopy. In this case, the cell monolayer was exposed to 100 nm PS-COOH NPs (100 μg/mL) for 10 min, then washed three times with PBS solution. Fresh NP-free culture medium was added to the sample, which was immediately imaged on the microscope in TIRF mode.

Dual-color TIRFM visualization of cell membrane and transferrin was performed on a spinning-disk confocal microscopy system consisting of a CSU22 spinning-disk unit (Yokogawa Electric Corporation) and an Andor iXon3 885 EMCCD camera (Andor, Belfast, UK), mounted on an inverted fully motorized Olympus IX81 microscope body (Olympus Corporation, Tokyo, Japan) with climate control chamber. The transferrin protein was excited with a 488 nm laser line and CellMask with a 561 nm laser line. A CFI Plan Apo TIRF 100×/1.49 WD = 0.12 mm oil immersion objective was used (Olympus). Images were acquired using Andor iQ2 software and processed using Imaris imaging software (Bitplane AG, Zurich, Switzerland).

Nanoparticle Translocation and Lysosomal Accumulation Quantification. Twenty-five consecutive three-dimensional images ("*z*-stacks") were obtained using spinning-disk confocal fluorescence microscopy of several different fields of view (size 70 μm × 70 μm) of the same culture. Nanoparticles and lysosomes (where applicable) were identified and followed over time using commercially available image analysis software (Imaris; Bitplane AG, Zurich, Switzerland). Nanoparticles in lysosomes were quantified as identified nanoparticles 0.5 μm from a lysosome, while nanoparticles were considered having translocated if immobile at the lower (basolateral) cell membrane for the majority (objects are sometimes missed in a few frames) of the 25 consecutive images.

The total number of nanoparticles as well as the number of nanoparticles translocated/in lysosomes was quantified in each field of view and then averaged over fields of view. Due to the low number of fields of view that can be conveniently imaged, we assessed the robustness of our averages by evaluating how the averages changed with the number of fields of view taken into account in calculating the average. In other words, we calculated the average for the first two fields of view, for the first three fields of view, *etc.*, separately. If the average does not change considerably after a certain minimum number of fields of view have been taken into account, then this suggests that the average would not change considerably if *all* fields of view would be taken into account. If this is the case, then the average is obviously representative of the culture.

Electron Microscopy. hCMEC/D3 cell monolayers grown on 0.4 μm PET Transwell membranes were exposed for 4 h to a 100 μg/mL nanoparticle dispersion. After three washes with PBS, the cell monolayers were fixed with glutaraldehyde (2.5% v/v) at room temperature for 1 h in Sorensen's phosphate buffer and postfixed for another 1 h in 1 g/mL osmium tetroxide in 0.05 M potassium phosphate buffer. The samples were rinsed in Sorensen's phosphate buffer and dehydrated by incubation in 30%, 50%, 70%, 90%, and 100% (v/v) ethanol solutions. Next, cells were immersed in an ethanol/Epon (1:1 v/v) mixture for 1 h before being transferred to pure Epon and embedded at 37 °C for 2 h. The final polymerization was carried out at 65 °C for 24 h. Ultrathin sections of 80 nm, obtained with a diamond knife using a Leica U6 ultramicrotome, were mounted on copper grids and stained with 2% uranyl acetate and 0.4% lead citrate before being examined with a FEI TECNAI transmission electron microscope (FEI Company, Hillsboro, OR, USA).

Transport Assay. The *in vitro* blood–brain system was prepared on a 12-well plate on a collagen-coated PTFE Transwell membrane (1.12 cm^2, 0.4 μm pore size, Corning, NY, USA). For transport experiments, hCMEC/D3 cells were seeded in 0.5 mL of assay medium at a density of 5×10^4 cells per filter in the apical compartment and 1.5 mL of assay medium in the basolateral compartment. The cell medium was changed twice a week. Transport assays were conducted 7 days post Transwell seeding. Both apical and basolateral chambers were washed twice with assay medium directly before experiments began. Transport study setup involved a 0.5 mL assay medium application to the Transwell apical compartment containing FITC-transferrin protein (25 μg/mL). The basolateral compartment contained 1.5 mL of assay medium, and Transwell membranes were placed in an orbital shaker (Titramax 1000, Heidolph, Schwabach, Germany) at 37 and 4 °C. Samples of 100 μL of assay medium were removed from the basolateral compartment every hour (up to a total of 4 h) and aliquoted onto black, flat-bottomed, 96-well plates (Corning). The 100 μL sample was replaced with fresh assay medium after each sampling. The fluorescence of FITC-transferrin protein was determined using a fluorimeter (Varioskan Flash, Thermo Fischer Scientific, Waltham, MA, USA) with an excitation/emission wavelength of 490/515 nm. A standard curve of fluorescence was calculated in order to determine sample concentration.

Conflict of Interest: The authors declare no competing financial interest.

Acknowledgment. Funding for this project has been generously provided by EU FP7 *via* the small collaborative project NeuroNano (NNP4-SL-2008-214547) and the small collaborative project NanoTransKinetics (NMP4-2010-EU-US-266737); by the INSPIRE (Integrated NanoScience Platform for IREland) program funded by the Irish Government's Programme for Research in Third Level Institutions, Cycle 4, National Development Plan 2007-2013; and by Science Foundation Ireland (09/RFP/MTR2425). Additionally it is based upon works supported by Science Foundation Ireland (SFI/SRC/B1155 and 12/IA/1422), EU FP7, *via* the Marie-Curie Initial Training Network PathChooser (PITN-GA-2013-608373) and the ESF Research Networking Programme EpitopeMap. J. Simpson and the imaging facilities at the School of Biology in University College Dublin are kindly acknowledged for assistance with imaging. Use of the Conway Institute Imaging Facility (University College Dublin) is also acknowledged. E. Mahon performed the fluorescent labeling of FITC-transferrin. D. Hudecz and L. Rocks are acknowledged for auxiliary experimental validation of the model. Endothelial hCMEC/D3 cells were provided by P.-O. Couraud, I. A. Romero, and B. Weksler.

Supporting Information Available: Estimate of the flux through holes and comparison with that through cells. Validation of the *in vitro* blood–brain barrier model morphology and functionality. *In vitro* blood–brain barrier model imperfections and limitations. Quantification of 40 and 100 nm PS-COOH nanoparticle translocation and lysosomal accumulation in the *in vitro* blood-brain barrier model. Real-time imaging of nanoparticle translocation through the *in vitro* blood–brain barrier model captured using TIRFM. Disruption of the *in vitro* blood–brain barrier model: an indication for the nanoparticles adhering to the glass below the barrier. Internalization of transferrin from the basolateral side in the *in vitro* blood–brain barrier model. This material is available free of charge *via* the Internet at http://pubs.acs.org.

REFERENCES AND NOTES

1. Abbott, N. J.; Rönnbäck, L.; Hansson, E. Astrocyte-Endothelial Interactions at the Blood-Brain Barrier. *Nat. Rev. Neurosci.* **2006**, *7*, 41–53.
2. Strazielle, N.; Ghersi-Egea, J. F. Physiology of Blood-Brain Interfaces in Relation to Brain Disposition of Small Compounds and Macromolecules. *Mol. Pharmaceutics* **2013**, *10*, 1473–1491.
3. Rejman, J.; Oberle, V.; Zuhorn, I. S.; Hoekstra, D. Size-Dependent Internalization of Particles *via* the Pathways of Clathrin- and Caveolae-Mediated Endocytosis. *Biochem. J.* **2004**, *377*, 159–169.
4. Chithrani, B. D.; Ghazani, A. A.; Chan, W. C. Determining the Size and Shape Dependence of Gold Nanoparticle Uptake into Mammalian Cells. *Nano Lett.* **2006**, *6*, 662–668.
5. Salvati, A.; Åberg, C.; dos Santos, T.; Varela, J.; Pinto, P.; Lynch, I.; Dawson, K. A. Experimental and Theoretical Comparison of Intracellular Import of Polymeric Nanoparticles and Small Molecules: Toward Models of Uptake Kinetics. *Nanomedicine (N. Y., NY, U. S.)* **2011**, *7*, 818–826.
6. Oberdörster, G.; Oberdörster, E.; Oberdörster, J. Nanotoxicology: An Emerging Discipline Evolving from Studies of Ultrafine Particles. *Environ. Health Perspect.* **2005**, *113*, 823–839.
7. Kreuter, J. Nanoparticulate Systems for Brain Delivery of Drugs. *Adv. Drug Delivery Rev.* **2012**, *64*, (Supplement), 213–222.
8. Begley, D. J. Delivery of Therapeutic Agents to the Central Nervous System: The Problems and the Possibilities. *Pharmacol. Ther.* **2004**, *104*, 29–45.
9. Pardridge, W. M. Blood-Brain Barrier Delivery. *Drug Discovery Today* **2007**, *12*, 54–61.
10. Andrieux, K.; Garcia-Garcia, E.; Kim, H. R.; Couvreur, P. Colloidal Carriers: A Promising Way to Treat Central Nervous System Diseases. *J. Nanoneurosci.* **2009**, *1*, 17–34.
11. Kreyling, W. G.; Semmler-Behnke, M.; Seitz, J.; Scymczak, W.; Wenk, A.; Mayer, P.; Takenaka, S.; Oberdörster, G. Size Dependence of the Translocation of Inhaled Iridium and Carbon Nanoparticle Aggregates from the Lung of Rats to the Blood and Secondary Target Organs. *Inhalation Toxicol.* **2009**, *21* (Supplement I), 55–60.
12. Oberdörster, G.; Sharp, Z.; Atudorei, V.; Elder, A.; Gelein, R.; Kreyling, W.; Cox, C. Translocation of Inhaled Ultrafine Particles to the Brain. *Inhalation Toxicol.* **2004**, *16*, 437–445.
13. Zensi, A.; Begley, D.; Pontikis, C.; Legros, C.; Mihoreanu, L.; Wagner, S.; Buchel, C.; von Briesen, H.; Kreuter, J. Albumin Nanoparticles Targeted with Apo E Enter the CNS by Transcytosis and Are Delivered to Neurones. *J. Controlled Release* **2009**, *137*, 78–86.
14. Kim, H. R.; Gil, S.; Andrieux, K.; Nicolas, V.; Appel, M.; Chacun, H.; Desmaele, D.; Taran, F.; Georgin, D.; Couvreur, P. Low-Density Lipoprotein Receptor-Mediated Endocytosis of Pegylated Nanoparticles in Rat Brain Endothelial Cells. *Cell. Mol. Life Sci.* **2007**, *64*, 356–364.
15. Wagner, S.; Zensi, A.; Wien, S. L.; Tschickardt, S. E.; Maier, W.; Vogel, T.; Worek, F.; Pietrzik, C. U.; Kreuter, J.; von Briesen, H. Uptake Mechanism of ApoE-Modified Nanoparticles on Brain Capillary Endothelial Cells as a Blood-Brain Barrier Model. *PLoS One* **2012**, *7*, e32568.
16. Kreuter, J.; Shamenkov, D.; Petrov, V.; Ramge, P.; Cychutek, K.; Koch-Brandt, C.; Alyautdin, R. Apolipoprotein-Mediated Transport of Nanoparticle-Bound Drugs across the Blood-Brain Barrier. *J. Drug Targeting* **2002**, *10*, 317–325.
17. Reimold, I.; Domke, D.; Bender, J.; Seyfried, C. A.; Radunz, H. E.; Fricker, G. Delivery of Nanoparticles to the Brain Detected by Fluorescence Microscopy. *Eur. J. Pharm. Biopharm.* **2008**, *70*, 627–632.
18. Ulbrich, K.; Hekmatara, T.; Herbert, E.; Kreuter, J. Transferrin- and Transferrin-Receptor-Antibody-Modified Nanoparticles Enable Drug Delivery across the Blood-Brain Barrier (BBB). *Eur. J. Pharm. Biopharm.* **2009**, *71*, 251–256.
19. Chang, J.; Jallouli, Y.; Kroubi, M.; Yuan, X. B.; Feng, W.; Kang, C. S.; Pu, P. Y.; Betbeder, D. Characterization of Endocytosis of Transferrin-Coated PLGA Nanoparticles by the Blood-Brain Barrier. *Int. J. Pharm. (Amsterdam, Neth.)* **2009**, *379*, 285–292.
20. Kumar, P.; Wu, H.; McBride, J. L.; Jung, K. E.; Kim, M. H.; Davidson, B. L.; Lee, S. K.; Shankar, P.; Manjunath, N. Transvascular Delivery of Small Interfering RNA to the Central Nervous System. *Nature (London, U. K.)* **2007**, *448*, 39–43.
21. Demeule, M.; Regina, A.; Che, C.; Poirier, J.; Nguyen, T.; Gabathuler, R.; Castaigne, J. P.; Beliveau, R. Identification and Design of Peptides as a New Drug Delivery System for the Brain. *J. Pharmacol. Exp. Ther.* **2008**, *324*, 1064–1072.
22. Martins, S.; Tho, I.; Reimold, I.; Fricker, G.; Souto, E.; Ferreira, D.; Brandl, M. Brain Delivery of Camptothecin by Means of Solid Lipid Nanoparticles: Formulation Design, *in Vitro* and *in Vivo* Studies. *Int. J. Pharm. (Amsterdam, Neth.)* **2012**, *439*, 49–62.
23. Gabathuler, R. Approaches to Transport Therapeutic Drugs across the Blood-Brain Barrier to Treat Brain Diseases. *Neurobiol. Dis.* **2010**, *37*, 48–57.
24. Monopoli, M. P.; Åberg, C.; Salvati, A.; Dawson, K. A. Biomolecular Coronas Provide the Biological Identity of Nanosized Materials. *Nat. Nanotechnol.* **2012**, *7*, 779–786.
25. Salvati, A.; Pitek, A. S.; Monopoli, M. P.; Prapainop, K.; Baldelli Bombelli, F.; Hristov, D. R.; Kelly, P. M.; Åberg, C.; Mahon, E.; Dawson, K. A. Transferrin-Functionalized Nanoparticles Lose Their Targeting Capabilities When a Biomolecule Corona Adsorbs on the Surface. *Nat. Nanotechnol.* **2013**, *8*, 137–143.
26. Weksler, B. B.; Subileau, E. A.; Perriere, N.; Charneau, P.; Holloway, K.; Leveque, M.; Tricoire-Leignel, H.; Nicotra, A.; Bourdoulous, S.; Turowski, P.; *et al*. Blood-Brain Barrier-Specific Properties of a Human Adult Brain Endothelial Cell Line. *FASEB J.* **2005**, *19*, 1872–1874.
27. Kim, J. A.; Åberg, C.; Salvati, A.; Dawson, K. A. Role of Cell Cycle on the Cellular Uptake and Dilution of Nanoparticles in a Cell Population. *Nat. Nanotechnol.* **2012**, *7*, 62–68.
28. Sandin, P.; Fitzpatrick, L. W.; Simpson, J. C.; Dawson, K. A. High-Speed Imaging of Rab Family Small GTPases Reveals

Rare Events in Nanoparticle Trafficking in Living Cells. *ACS Nano* **2012**, *6*, 1513–1521.
29. Nic Raghnaill, M.; Bramini, M.; Ye, D.; Couraud, P.-O.; Romero, I. A.; Weksler, B.; Åberg, C.; Salvati, A.; Lynch, I.; Dawson, K. A. Paracrine Signalling of Inflammatory Cytokines from an *in Vitro* Blood Brain Barrier Model upon Exposure to Polymeric Nanoparticles. *Analyst (Cambridge, U. K.)* **2014**, *139*, 923–930.
30. Vu, K.; Weksler, B.; Romero, I.; Couraud, P. O.; Gelli, A. Immortalized Human Brain Endothelial Cell Line hCMEC/D3 as a Model of the Blood-Brain Barrier Facilitates *in Vitro* Studies of Central Nervous System Infection by Cryptococcus Neoformans. *Eukaryotic Cell* **2009**, *8*, 1803–1807.
31. Nic Ragnaill, M.; Brown, M.; Ye, D.; Bramini, M.; Callanan, S.; Lynch, I.; Dawson, K. A. Internal Benchmarking of a Human Blood-Brain Barrier Cell Model for Screening of Nanoparticle Uptake and Transcytosis. *Eur. J. Pharm. Biopharm.* **2011**, *77*, 360–367.
32. Fishman, J. B.; Rubin, J. B.; Handrahan, J. V.; Connor, J. R.; Fine, R. E. Receptor-Mediated Transcytosis of Transferrin across the Blood-Brain Barrier. *J. Neurosci. Res.* **1987**, *18*, 299–304.
33. Ye, D.; Nic Raghnaill, M.; Bramini, M.; Mahon, E.; Åberg, C.; Salvati, A.; Dawson, K. A. Nanoparticle Accumulation and Transcytosis in Brain Endothelial Cell Layers. *Nanoscale* **2013**, *5*, 11153–11165.
34. Conner, S. D.; Schmid, S. L. Regulated Portals of Entry into the Cell. *Nature (London, U. K.)* **2003**, *422*, 37–44.
35. Iversen, T. G.; Skotland, T.; Sandvig, K. Endocytosis and Intracellular Transport of Nanoparticles: Present Knowledge and Need for Future Studies. *Nano Today* **2011**, *6*, 176–185.
36. Bhabra, G.; Sood, A.; Fisher, B.; Cartwright, L.; Saunders, M.; Evans, W. H.; Surprenant, A.; Lopez-Castejon, G.; Mann, S.; Davis, S. A.; *et al*. Nanoparticles Can Cause DNA Damage across a Cellular Barrier. *Nat. Nanotechnol.* **2009**, *4*, 876–883.
37. Sood, A.; Salih, S.; Roh, D.; Lacharme-Lora, L.; Parry, M.; Hardiman, B.; Keehan, R.; Grummer, R.; Winterhager, E.; Gokhale, P. J.; *et al*. Signalling of DNA Damage and Cytokines across Cell Barriers Exposed to Nanoparticles Depends on Barrier Thickness. *Nat. Nanotechnol.* **2011**, *6*, 824–833.